scan angle corresponding to the location of the beacon. Consequently, we conclude that the self-survey technique accurately coheres a nonrigid array.

The radiation pattern was measured, after self-survey and beam forming, for three configurations of the flexing array and for numerous beam-pointing directions. A typical radiation pattern focused at broadside (beam-forming angle = 0°) is shown in Fig. 2. The pointing accuracy is evident. The width of the main beam is consistent with the size of the array [5, p. 40]. The relatively high sidelobe level is in no way a consequence of self-survey, but rather the level expected of an array containing so few elements [5, p. 142]. Comparison of the radiation patterns for the different array configurations showed variations in the height and placement of particular sidelobes; however, the average sidelobe level was not affected by array flexure.

The main-beam gain and pointing error measured relative to a perfectly cohered beam was recorded as a function of scan angle from broadside for the three array configurations. The gain loss and squared pointing error were averaged over all scan angles within the spread of the beacons and over all three array configurations to obtain an average gain loss of $L = -0.061$ dB and an rms pointing error of 0.021°. This pointing error is very small, and the gain loss is approximately the same as the predicted value.

The gain loss is plotted as a function of pointing angle for several trials in [6]. The shapes of the curves are as predicted by the analysis in [3]. That is, there is little gain loss for pointing angles within the spread of the beacons; the gain loss rises somewhat for pointing angles near the edges of the spread and becomes large for angles outside the spread.

The tolerance theory in [3] indicates that beacon angle measurement errors should cause a pure beam-pointing error in a nearly linear self-cohered array. In order to test that theory, we repeated the self-survey processing a number of times for three array configurations, using beacon angle estimates to which known errors were added. The main-beam characteristics were measured after self-surveying with each different combination of beacon angle errors. A typical result is shown in Fig. 3. (The errors in the beacon angle measurements are shown in the figure.) The gain plot is almost identical with the gain plot in the absence of beacon angle errors (see [6]), verifying the prediction that the error would be a pure pointing error. The mean beacon angle measurement error for Fig. 3 is positive (corresponding to a negative mean beacon placement error). Consequently, we would expect the mean pointing error to be negative as shown in the figure.

The tolerance theory in [3] predicts that the variance in pointing error will be roughly equal to the rms of the beacon angle errors for pointing angles within the spread of the beacons but will be large for pointing angles outside the spread. The pointing error for an individual trial (Fig. 3) need not follow this pattern. We obtained the pointing error as a function of pointing angle for eight different sets of beacon angle measurement errors for each of three array configurations. We normalized the pointing error plot for each trial by the rms of the beacon angle errors for that trial, then determined the mean square pointing error as a function of the pointing angle. The resulting curve was in close agreement with the predicted curve of pointing error variance [6]; that is, the values of the normalized curve were slightly less than unity for pointing angles within the 40° spread of the beacons but large outside the spread.

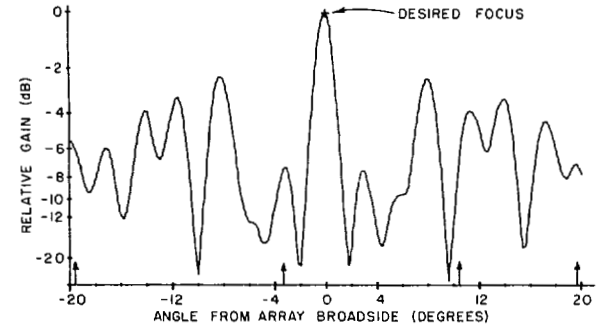

Fig. 2. Typical radiation pattern after self-survey. Vertical arrows indicate beacon angles.

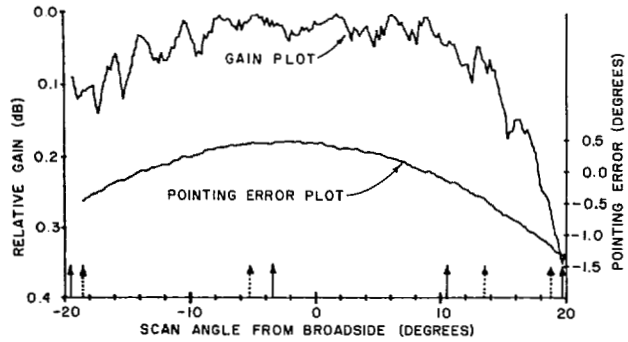

Fig. 3. Effect on focused main beam of beacon angle measurement errors. Errors are 1°, −2°, 3°, −1°. Solid arrows indicate accurate beacon angles. Dotted arrows indicate error-corrupted angles.

REFERENCES

[1] B. D. Steinberg, "Design approach for a high-resolution microwave imaging radio camera," *J. Franklin Inst.*, vol. 296, Dec. 1973.

[2] C. N. Dorny and T. L. Lim, "A large thinned array for shipboard radar," in *EASCON 1978 Conf. Rec.*

[3] C. N. Dorny, "A self-survey technique for self-cohering of antenna systems," *IEEE Trans. Antennas Propagat.*, vol. AP-26, pp. 877–881, Nov. 1978.

[4] D. Carlson, "Four-element array with signal processing," Valley Forge Res. Center, Univ. of Pennsylvania, Philadelphia, PA, QPR 20, Feb. 1977, pp. 26–29.

[5] B. D. Steinberg, *Principles of Aperture and Array System Design*. New York: Wiley, 1976.

[6] C. N. Dorny and B. S. Meagher, Jr., "Cohering of an experimental nonrigid array by self-survey," Valley Forge Res. Center, Univ. of Pennsylvania, Philadelphia, PA, Rep. UP-VFRC-19-78, Nov. 1978.

A New Approach to Active Antenna Design

ERNST H. NORDHOLT AND DURK VAN WILLIGEN

Abstract—**Design considerations for wide-band active antenna circuits for frequencies up to 30 MHz are presented. High performance is obtained by using unusual amplifier types having a**

Manuscript received May 22, 1979; revised June 2, 1980.

The authors are with the Department of Electrical Engineering, Delft University of Technology, Delft, The Netherlands.

0018-926X/80/1100-0904$00.75

virtually grounded input electrode of the input active device, and a large amount of negative feedback over several stages. The realized antennas with a physical length of 0.5 m have a flat frequency response from 5 kHz to 30 MHz and extremely low distortion (second-order intercept >+70 dBm, third-order intercept >+50 dBm). The antennas are thoroughly protected against statics; without sacrificing the high dynamic range. Output power levels up to +28 dBm can be handled. The electric field strength may exceed 10 V/m. The equivalent input noise field strength amounts to about 25 nV/m$\sqrt{\text{Hz}}$.

I. INTRODUCTION

An undisturbed reception of radio signals in the frequency region 10 kHz–30 MHz is strongly hampered by (external) atmospheric, man-made, and galactic noise. It is obvious that there is no reason to strive for a noise contribution of the receiving system that is far below the received external noise.

Even with short–very high impedance–antennas ($1 \ll \lambda$) it appears to be possible to maintain the external signal-to-noise ratio, provided that a specially designed amplifier is inserted between antenna and receiver. Following common practice, we will indicate such a combination of an antenna and an amplifier directly connected to it as an active antenna [1], [2]. Because of the small physical dimensions of active antennas, their application is very attractive in mobile receiving systems and in antenna arrays.

An active antenna can have various additional advantages.

- Its transfer function can be made broad-band and frequency independent and can be accurately fixed.
- Its output impedance can be accurately matched to the characteristic impedance of the cable to the receiver.

Because an amplifier forms a part of the active antenna, noise and distortion products are inevitably added to the received signals. Design efforts must therefore be focused on minimizing these contaminating signals and maximizing signal-handling capability.

Amplifier noise minimization offers the possibility of reducing antenna length. The reduction of intermodulation distortion and the enlargement of the signal-handling capability increase the suitability of active antennas on locations where strong interfering signals are present. Other important design aspects are the accuracy of the antenna transfer function (for application in antenna arrays) and the protection against statics.

In this communication we will present design considerations for broad-band active antennas for the 10 kHz–30 MHz range. The resulting configurations have significantly better properties than those reported until now. The major improvements are consequences of a new approach that does not use basically new amplifier techniques, but that breaks with a current prejudice that implies that the input impedance of the active-antenna amplifier should be high for optimum performance [3]. The keys to the improvements are as follows:

- the application of a large amount of negative feedback around several cascaded stages, instead of the use of cascaded stages with local feedback, and
- a virtual grounding of the input electrode of the input active device by special types of feedback at the input, allowing protection without degradation of the linearity and the accuracy of the antenna transfer function.

An additional improvement can be obtained by applying two negative feedback loops to prevent the loss of output signal power.

II. DESCRIPTION OF THE RECEIVING SYSTEM

The active antennas to be dealt with are composed of a short passive antenna rod ($1 \ll \lambda$) and an amplifier directly connected to it. The antenna rod is assumed to be placed on a supporting structure. The amplifier ground may therefore carry a substantial common-mode voltage. The virtual ground mentioned above refers to the differential input signal of the amplifier. The influence of supporting structures on the antenna parameters has been described by Lindenmeier [3]. Fig. 1 shows a complete receiving system. The equivalent circuit of the passive antenna is given in this figure. E is the electric field strength, h_{eff} is the effective height, and C_a represents the antenna impedance.

The function of the active antenna is to convert accurately the information present in the electromagnetic field into an electric power delivered to the receiver containing the same information without the addition of contaminating signals such as noise or intermodulation products.

Referring to Fig. 1, the design goal can be formulated alternatively: the transfer function $U_{RX}/E = h_{ae}$ (the effective active antenna height) must be realized as noise-free, linearly, and accurately as possible. The last requirement in particular refers to the application of active antennas in antenna arrays.

Furthermore, a protection against "statics" must be attended to. For this purpose, low noise, high speed, high current diodes are suitable, and it will be assumed that these diodes are placed in parallel with the input electrodes of the input active device.

The output impedance Z_0 of the amplifier is conveniently chosen to be equal to the generally accepted characteristic impedance of 50 Ω. In consumer applications such as car radios this last requirement can be abandoned, giving some relief with respect to signal-handling capability.

III. THE AMPLIFIER SIGNAL-TRANSFER FUNCTION

The realization of highly accurate and linear transfer functions requires the application of negative feedback with large (open) loop gain. Optimum results can be obtained if the loop gain is made as large as possible, but still consistent with bandwidth and stability requirements. Therefore, feedback is preferably applied around several stages (overall feedback), provided that the poles of the loop transfer function are sufficiently manageable.

Various types of feedback can be considered. An important design consideration is that those types of input feedback are preferred that do not seriously degrade the noise performance limits set by the input active device of the amplifier. Moreover, the feedback should force the input electrode of the input active device to ground potential ("virtual ground"), so that the input protection diodes do not disturb the linearity nor the accuracy of the antenna transfer function.

Configurations with floating input ports (such as conventional voltage amplifiers and voltage followers) are inferior because of their voltage dependent and inaccurately known input capacitances, composed of the input-device feedback capacitance, the capacitance of the protection diodes, and some wiring capacitance. The configurations given in Fig. 2 meet the above condition of a virtual ground, and have frequency independent transfer functions in addition. These are given for a sufficiently large loop gain and with $Z_0 = Z_l$ by

$$A_{u\infty} = U_l/U_a = -\tfrac{1}{2}\, C_a/C_f \qquad \text{(a)}$$

$$A_{u\infty} = U_l/U_a = \tfrac{1}{2}\, n. \qquad \text{(b)}$$

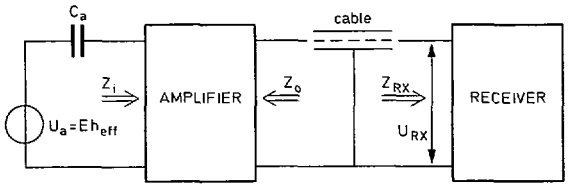

Fig. 1. Receiving system with active antenna. U_a is open (passive) antenna voltage; C_a is (passive) antenna impedance.

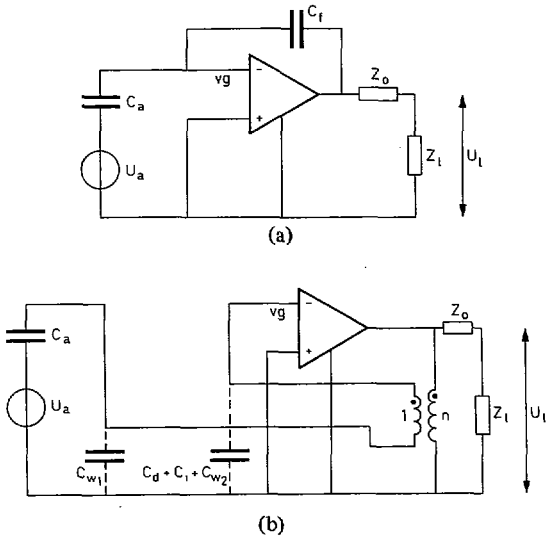

Fig. 2. Active antenna amplifier configurations with frequency-independent transfer functions and virtually grounded input electrode (vg) of input active device.

The configuration of Fig. 2(a) has a low input impedance and the transfer function is, therefore, largely insensitive to parasitic impedances at the antenna footpoint. The configuration of Fig. 2(b) has a high input impedance. The (small) wiring capacitance C_{w1} may have some influence on the transfer function.

The type of feedback at the output should preferably not reduce the signal-handling capability. A combination of shunt and series feedback is advantageous for realizing the desired 50-Ω output impedance, thus avoiding the usual output power loss of 3 dB caused by the 50-Ω series or shunt impedances [4]. Fig. 3 gives two basic configurations. Their transfer properties in the case of infinite loop gain are summarized in the figure legends.

The so-called transimpedance amplifier of Fig. 2(a) is attractive in spite of its output power loss in the 50-Ω series resistance at the output because no transformers are needed. It is particularly suitable for applications in low-cost car-radio antennas. Moreover, it lends itself to manufacture as an integrated circuit.

IV. NOISE CONSIDERATIONS

The noise of the total receiving system is composed of three distinguishable contributions:

- the external noise generated in the passive antenna, which can be estimated for a specified time and location from the CCIR report 322 [5] and can be characterized by the external-noise field strength e_{en}, resulting in an antenna voltage $u_{aen} = e_{en}h_{eff}$;
- the noise generated in the amplifier, which can directly be expressed in an equivalent antenna noise voltage u_{ea} when the antenna impedance is known;
- the noise generated in the receiver, characterized by its noise figure F_{RX}. It can conveniently be converted into an equivalent antenna noise voltage u_{eRX} as well.

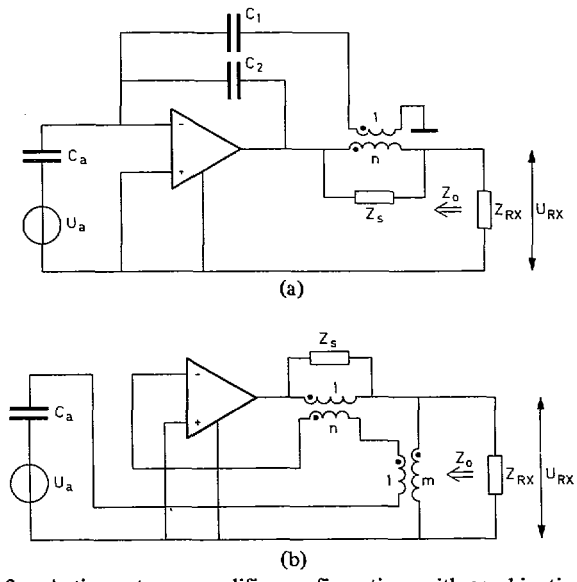

Fig. 3. Active antenna amplifier configurations with combinations of series and shunt feedback at output in order to avoid output power loss. (a) For $Z_0 = Z_s(1 + nC_1/C_2) = Z_{RX}$: $U_{RX}/U_a = -C_a/2C_2$. (b) For $Z_0 = Z_s \cdot n \cdot m = Z_{RX}$: $U_{RX}/U_a = m/2$.

The total power density spectrum of the equivalent antenna noise voltage can be written as the sum of the converted spectra:

$$S(u_{eq.tot}) = S(u_{aen}) + S(u_{eRX}) + S(u_{ea}).$$

The relative shares of these noise contributions depend on various parameters of the system, such as the length of the antenna, the receiving frequency, the gain of the amplifier, and the noise parameters of the input device of the amplifier. We will deal successively with the various contributions.

A. Noise Contribution of the Amplifier

The active system can be characterized by two equivalent input noise sources u_{eq} and i_{eq}. The equivalent antenna noise voltage u_{ea} can be determined by converting the current source i_{eq} into a voltage source. Supposing that the sources u_{eq} and i_{eq} are uncorrelated, we find

$$S(u_{ea}) = S(u_{eq}) + S(i_{eq})\frac{1}{\omega^2 {C_a}^2}. \quad (1)$$

From this expression it follows that the influence of the equivalent current source is larger at lower frequencies and for higher antenna impedances.

For short antennas in the VLF and LF frequency band, $S(i_{eq})$ must be extremely small, and the field effect transistor (FET) is therefore the obvious choice for the input device. Fig. 4 shows a simple equivalent circuit of the junction FET with its noise sources i_{ig}, i_g, i_d, and i_{df}.

In addition, the load impedance Z_l and its associated noise source i_l are shown, together with the input noise sources u_{2eq} and i_{2eq} of the second amplifier stage. The antenna is supposed to be directly connected to the FET.

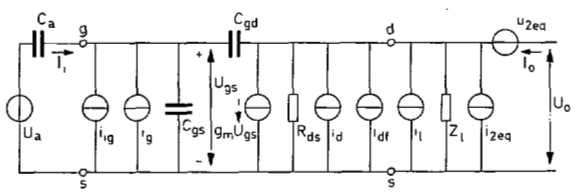

Fig. 4. Equivalent circuit of junction FET input stage with noise sources of FET, load, and second stage.

The feedback network components are not taken into account for the time being. The thermal channel noise of the FET is represented by the sources i_{ig} and i_d. It can be shown that the influence of the induced gate noise i_{ig} can be disregarded in wide-band amplifiers [6]. The spectrum of i_d is given by $S(i_d) = 4kTcg_m$, where the constant c has a value between 1 and 1.5 [7]. The sources i_g and i_{df}, representing the shot noise of the gate leakage current and the excess noise, respectively, only play roles at very low frequencies. Furthermore, noise currents will be added at the input by the presence of bias and protection components. We will give them attention separately.

The current sources i_d, i_l, and i_{2eq} can be combined into one source i_0 whose spectrum is given by

$$S(i_0) = S(i_d) + S(i_l) + S(i_{2eq}).$$

This source and the source u_{2eq} can be transformed into an equivalent noise voltage u_{ea} with a spectrum:

$$S(u_{ea}) = \frac{S(i_0)}{g_m^2}\left(\frac{C_{gs} + C_{gd} + C_a}{C_a}\right)^2 + S(u_{2eq})\left|\frac{1}{A_{u0}} + \frac{1}{j\omega C_a}\cdot\frac{1}{Z_{t0}}\right|^2, \quad (2)$$

under the reasonable assumption that u_{2eq} and i_{2eq} can be considered uncorrelated. When the first amplifier stage is a common-source stage, A_{u0} and Z_{t0} can be defined with reference to Fig. 4 as

$$A_{u0} = \frac{U_0}{U_{gs}} \quad \text{and} \quad Z_{t0} = \frac{U_0}{I_i}.$$

The second term in (2) can easily be made very small for a second stage with a bipolar transistor as well as with a junction FET, provided that Z_l has a sufficiently large value. The equivalent input noise current of the second stage, however, may not be negligible when this stage is equipped with a bipolar transistor, because its bias current is necessarily large for realizing adequate signal-handling capabilities. Consequently, its input shot noise is large. A FET is advantageous in the second stage as well. The second-stage noise sources and the noise of the load impedance can generally be disregarded when a common-source input stage is used [6]. In that case, the minimum noise contribution of the amplifier becomes

$$S(u_{ea})_{min} = 4kTc\frac{1}{g_m}\left(\frac{C_{gs} + C_{gd} + C_a}{C_a}\right)^2. \quad (3)$$

In general, the feedback networks have some influence on the noise performance. In the transformer feedback case of Fig. 2(b), this influence is negligible because of the nonenergic (instantaneously lossless) feedback network [4].

In the configuration with shunt feedback at the input (Fig. 2(a)), the feedback capacitance C_f slightly deteriorates noise performance. As can be shown, it adds to the total capacitance in the numerator of (3). Parasitic shunt capacitance at the input (protection diodes) can be taken into account in the same way [4]. Similar considerations apply to the configurations of Fig. 3.

In the low frequency region, the influence of the noise of the leakage currents of the FET and the protection diodes, the thermal noise current of a bias resistor and the excess noise must be considered. In the case of a junction FET as the input device, the excess noise contribution can be disregarded. The other sources can be combined into one white noise current source i_g', producing an equivalent antenna voltage spectrum, given by

$$S(u_{ea.g'}) = S(i_g')\frac{1}{\omega^2 C_a^2} = \frac{4kT}{R_g'}\cdot\frac{1}{\omega^2 C_a^2}, \quad (4)$$

causing an enhancement of the amplifier noise at low frequencies. R_g' is an equivalent thermal noise resistance composed of the bias resistance and the equivalent thermal resistances of the leakage currents of the protection diodes and the FET.

The frequency ω_l for which this spectrum equals the FET thermal noise spectrum is given by

$$\omega_l^2 = \frac{g_m}{cR_{g'}(C_{gs} + C_{gd} + C_a)^2}.$$

Some typical values of circuit parameters are $c/g_m = 500\ \Omega$, $R_g' = 5\cdot10^8\ \Omega$, and $C_{gs} + C_{gd} + C_a = 15$ pF, resulting in $f_l \cong 20$ kHz. For shorter antennas this frequency will be higher.

It may be concluded that, for frequencies higher than f_l, the active antenna can be designed such that the amplifier noise contribution is determined only by the parameters of the FET in the input stage and by the antenna impedance. Feedback components and protection diodes only slightly deteriorate noise performance, because of some additional shunt capacitance at the input. The noise contribution of the bias resistance, protection diodes and gate leakage current dominate at very low frequencies. It cannot be neglected for antennas specially designed for the VLF band.

B. Noise Contribution of the Receiver

If the noise figure F_{RX} of the receiver is known and its source impedance, i.e., the amplifier output impedance, equals 50 Ω, the receiver noise can be represented by a voltage source in series with the receiver input, the spectrum of which is given by

$$S(u_{RX}) = (4kT \cdot 50)\, 10^{0.1(F_{RX})}.$$

This source can be transformed into an equivalent antenna voltage, by dividing it by the open voltage gain U_0/U_a of the amplifier.

For the configuration of Fig. 2(a), for example, the spec-

trum of the equivalent antenna noise voltage becomes

$$S(u_{eRX}) = S(u_{RX})\frac{C_f^2}{C_a^2}$$

A typical value of F_{RX} is $F_{RX} \cong 10$ dB, so that $S(u_{rx}) = 4kT(10 \cdot 50)$.

The ratio of C_f and C_a is preferably chosen so that $S(u_{eRX})$ can be disregarded with respect to the amplifier noise $S(u_{ea})$, which requires a sufficiently large active antenna transfer function. On the other hand, the amplifier gain cannot be made arbitrarily large because this conflicts with the required large signal-handling capability.

C. External Noise

In Fig. 5 a typical plot of the expected noise field strength for a certain time and location as calculated from CCIR data [5] is shown. Two curves are shown for the atmospheric noise with $F_{am} = 10$ dB and $F_{am} = 60$ dB. F_{am} is the external noise figure for $f = 1$ MHz. For its definition we refer to the CCIR report 322.

In Fig. 6, plots are given of the rms noise contribution of the receiving system as a function of the antenna capacitance and with the amplifier gain as a parameter for the configurations of Fig. 2. The noise figure of the receiver is supposed to have a value $F_{RX} \cong 10$ dB. For the input device of the amplifier the following parameter values are taken: $C_{gs} + C_{gd} = 5$ pF, $c/g_m = 400\ \Omega$.

To provide an impression of the required antenna length for a certain application we have plotted in the same figure the (rms) external noise contribution as a function of the antenna length for various frequencies, based on the plot of Fig. 10 with $F_{am} = 60$ dB. The antenna length and antenna capacitance are assumed to be related as $C_a/l_a = 10$ pF/m, which is about typical for antenna rods with $l \gg d$. From this plot it can be seen that very small antennas can be applied in the VLF region. For higher frequencies larger antennas or better input devices (high ω_T, low noise) are necessary to have external noise contributions of the same order of magnitude as the noise of the receiving system.

V. LINEARITY CONSIDERATIONS

The mere application of the proper types of feedback at input and output is not a sufficient measure for realizing a highly linear transfer function. Important prerequisites are a large magnitude of the loop gain and a high linearity of the loop transfer function. The realizable magnitude of the loop transfer function is largely determined by the transit frequencies of the available active devices and by the number of manageable poles in the loop transfer function.

The compensation techniques needed for a flat stable frequency response should reduce loop gain only in those frequency regions where a reduction is inevitable. Moreover, the compensation should be designed in such a way that it is not accompanied by a deterioration of the linearity of the loop transfer function. Balancing of the stages, especially of the output stage, can further improve linearity. The design of the active antennas presented in the next section is based on the above considerations [6].

VI. EXPERIMENTAL RESULTS

A. Circuits Description

In order to illustrate the fruitfulness of this new design approach, where the active part of the amplifier has a virtually grounded input electrode and a large amount of negative feedback over several stages is used, two different active antennas have been constructed. Fig. 7 shows the basic realizations. The amplifiers A and B can be inserted into the dashed framework. The surrounding circuitry accomplishes the input protection and the supply of dc power through the coax cable. The internal circuit of the amplifier is shown in Fig. 8. Heavily drawn lines indicate the signal path. Terminal numbers correspond to those of Fig. 7.

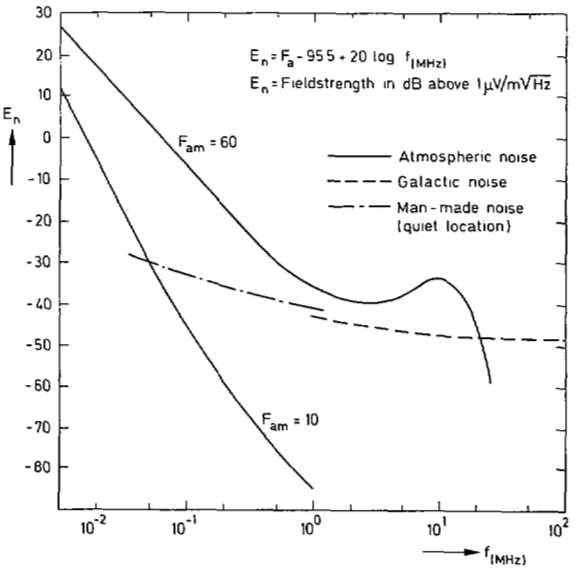

Fig. 5. Expected noise field strength for certain time and location.

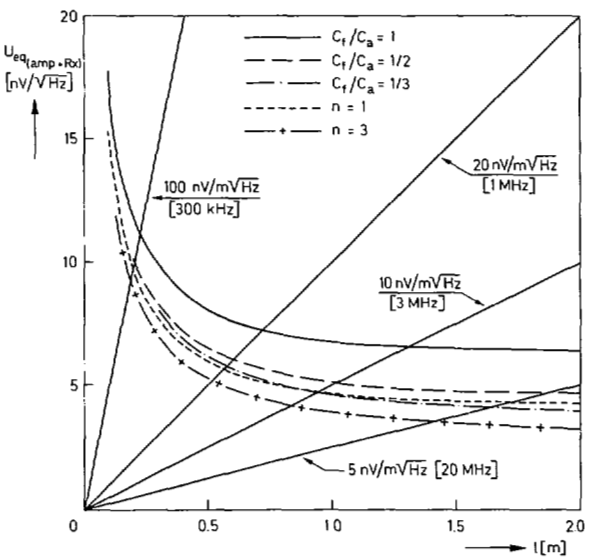

Fig. 6. Rms noise contribution of receiving system for configurations of Fig. 2 with amplifier gain (C_a/C_f or n) as parameter (curved lines). In addition, contribution of external noise is plotted as function of antenna length for various frequencies (straight lines).

B. Measurements

All measurements were made with a simulated antenna consisting of a voltage source in series with a 10-pF capacitor (Fig. 1). In Fig. 9 the noise and intermodulation performance of the active antennas is summarized. Second- and third-order intercept points and noise levels at the output are given. Furthermore, the intermodulation products and signal output power are given as functions of the electric field strength.

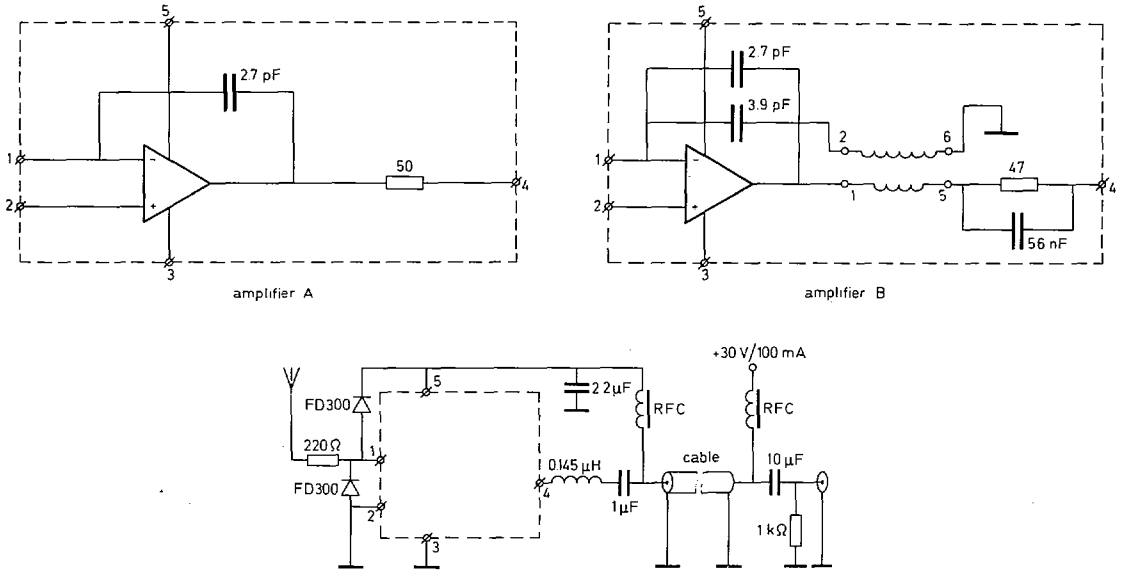

Fig. 7. Active antenna with two different amplifier circuits *A* and *B* with protection and dc supply circuitry.

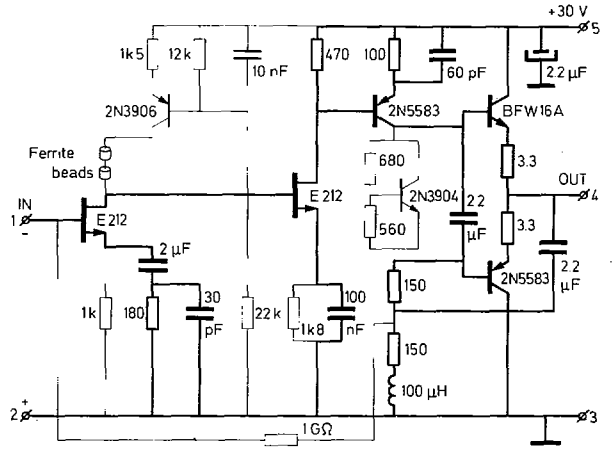

Fig. 8. Internal amplifier circuit. Numbers 1–5 correspond to those of Fig. 7.

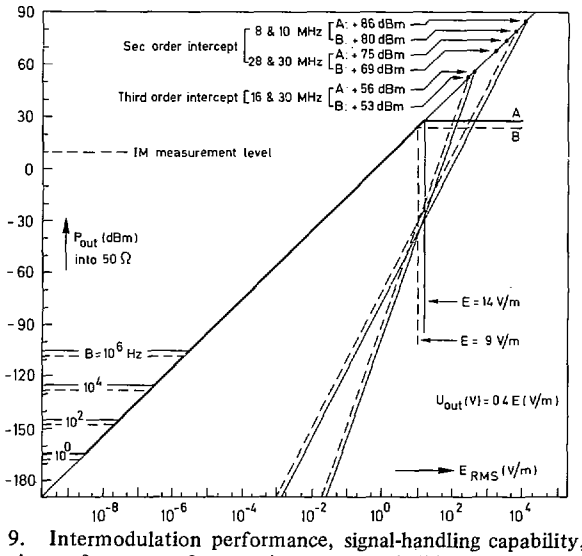

Fig. 9. Intermodulation performance, signal-handling capability, and noise performance of two active antennas. Solid lines: configuration *A*; dashed lines: configuration *B*.

Both antennas have physical lengths of 0.5 m and diameters of 30 mm. The effective active antenna length equals 0.4 m is constant within ±0.5 dB in the frequency range 5 kHz–30 MHz. In this frequency range VSWR $\leq$ 1.25. The protection circuit was tested by supplying over 10^6 1-cm sparks of a 10-kV automobile ignition coil directly to the active antenna input. This rather rough test did not harm the circuit in any way. The high-speed protection diodes do contribute about 1 dB to the noise level of the antenna.

VII. CONCLUSION

In this communication we have presented some design considerations for active antennas for frequencies below 30 MHz. It was pointed out that optimum performance can be obtained with amplifiers having the proper types of feedback at input and output so that the noise and distortion performance are not seriously degraded and the transfer function is accurately established. A virtually grounded input electrode of the input active device is required for optimum performance, and at the output a combination of series and shunt feedback is advantageous.

Measurement results were given, showing that these types of active antennas can be used on nearly every location because of their extremely low distortion and large admissible electric field strength (about 10 V/m), while they will outperform most receivers as far as dynamic range is concerned.

In cases where still larger field strengths must be handled, a reduction of the effective antenna legnth (h_{ae}) is necessary for a given supply voltage. The noise contribution of the receiver to the total system noise is enlarged in that case.

ACKNOWLEDGMENT

The authors are very indebted to Mr. Martin P. I. Huisman who constructed the antennas and who did numerous measurements.

REFERENCES

[1] H. H. Meinke, "Aktive Antennen," *Nachrichtentech. Z.*, 26, H. 8, pp. 361–362, 1973.

[2] H. Lindenmeier and G. Flachenecker, "Breitbandige transistorierte Empfangsantennen im Frequenzbereich zwischen 10 kHz und 10 MHz," *Nachrichtentech. F.*, vol. 45, pp. 140–145, 1972, Berlin-Charlottenburg: VDE-Verlage.
[3] H. Lindenmeier, "Die transistorierte Empfangsantenne mit kapazitive hochohmigen Verstärker als optimale Lösung für den Empfang niedriger Frequenzen," *Nachrichtentech. Z.*, 27, H. 11, pp. 411–418, 1974.
[4] E. H. Nordholt, "Classes and Properties of Multiloop Negative-Feedback Amplifiers," submitted to *IEEE Trans. Circuits Syst.*
[5] CCIR Rep. 322, Int. Telecommunication Union, Geneva, Switzerland, 1964.
[6] E. H. Nordholt, "The design of high-performance negative-feedback amplifiers," Ph.D. dissertation, Delft University of Technology, Delft, The Netherlands, 1980.
[7] C. D. Motchenbacher and F. C. Fitchen, *Low-Noise Electronic Design*. New York: Wiley, 1973, p. 102.

Radiation from Unsymmetrically Excited Elliptical Apertures

DAU-CHYRH CHANG AND W. V. T. RUSCH, FELLOW, IEEE

Abstract—**Expressions are derived for the field radiated by an unsymmetrically excited elliptical aperture which also encompass the special case of an unsymmetrically excited circular aperture. Tables and figures are presented for the case of symmetrical excitation and for a specific example of unsymmetrical excitations.**

I. ANALYSIS

The field radiated from an elliptical aperture of area $A = \pi ab$, major and minor semi-axes a and b, respectively (Fig. 1), and a cophasal aperture distribution $F(x, y)$ can be approximated by [1], [2]

$$U(R, \theta, \varphi) = \frac{j}{\lambda R} e^{-jkR} I \tag{1}$$

where

$$I = \iint F(x, y) e^{jk \sin\theta (x\cos\varphi + y \sin\varphi)} \, dx \, dy. \tag{2}$$

$$F(x, y) = \left[1 - \frac{x^2}{a^2} - \frac{y^2}{b^2}\right]^p \cos^2 \delta + \left[1 - \frac{x^2}{a^2} - \frac{y^2}{b^2}\right]^q \sin^2 \delta. \tag{3}$$

This generalized distribution function will have a null at the edge of the aperture and have elliptical amplitude contours everywhere when $p = q$. The parameters p and q can be varied to obtain a wide family of field distributions on the elliptical aperture. J. I. Glaser has analyzed the special case of an elliptical aperture with $p = q$ by a different method [3].

Letting

$$x = ar \cos \delta \tag{4a}$$

$$y = br \sin \delta \tag{4b}$$

Manuscript received February 24, 1980; revised July 7, 1980.
The authors are with the Department of Electrical Engineering, University of Southern California, Los Angeles, CA 90007.

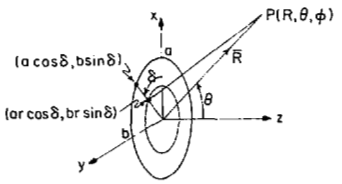

Fig. 1. Geometry of elliptical aperture.

where $0 \leqslant r \leqslant 1$ and $0 \leqslant \delta \leqslant 2\pi$, the distribution function becomes

$$F(x, y) = (1 - r^2)^p \cos^2 \delta + (1 - r^2)^q \sin^2 \delta. \tag{5}$$

Transforming the differential surface element by means of the Jacobian transformation:

$$dx dy = \begin{vmatrix} \frac{\partial x}{\partial r} & \frac{\partial x}{\partial \delta} \\ \frac{\partial y}{\partial r} & \frac{\partial y}{\partial \delta} \end{vmatrix} = abr dr d\delta \tag{6}$$

so that (2) becomes

$$I = \pi ab (I_p + I_q) \tag{7}$$

where [4]

$$I_p = \frac{2^p p! J_{p+1}(u)}{u^{p+1}} - \cos 2\alpha \left\{ \frac{2}{u^2} [1 - J_0(u)] - \frac{2^p p! J_{p+1}(u)}{u^{p+1}} - \sum_{j=0}^{p} \frac{2^j (j-1)! J_{j+1}(u)}{u^{j+1}} U(j-1) \right\} \tag{8a}$$

$$I_q = \frac{2^q q! J_{q+1}(u)}{u^{q+1}} + \cos 2\alpha \left\{ \frac{2}{u^2} [1 - J_0(u)] - \frac{2^q q! J_{q+1}(u)}{u^{q+1}} - \sum_{j=0}^{q} \frac{2^j (j-1)! J_{j+1}(u)}{u^{j+1}} U(j-1) \right\}. \tag{8b}$$

Thus,

$$\frac{I}{\pi ab} = \left[\frac{2^p p! J_{p+1}(u)}{u^{p+1}} + \frac{2^q q! J_{q+1}(u)}{u^{q+1}} + \cos 2\alpha \left\{ \left[\frac{2^p p! J_{p+1}(u)}{u^{p+1}} - \frac{2^q q! J_{q+1}(u)}{u^{q+1}} \right] + \left[\sum_{j=0}^{p} \frac{2^j (j-1)! J_{j+1}(u)}{u^{j+1}} U(j-1) - \sum_{j=0}^{q} \frac{2^j (j-1)! J_{j+1}(u)}{u^{j+1}} U(j-1) \right] \right\} \tag{9}$$

0018-926X/80/1100-0910$00.75 © 1980 IEEE